Changes are marked by red color

Enhancements of Airborne Particulate Arsenic over the Subtropical Free Troposphere: Impact by South Asian Biomass Burning

Yu-Chi Lin[1,2,3], Shih-Chieh Hsu[3], Chuan-Yao Lin[3], Shuen-Hsin Lin[3], Yi-Tang Huang[3], Yunhua Chang[1,2], Yan-Lin Zhang[1,2*]

[1.] *Yale-NUIST Center on Atmospheric Environment, Nanjing University of Information Science and Technology, Nanjing, Jiangsu, China.*

[2.] *Key Laboratory of Meteorological Disaster, Ministry of Education & Collaborative Innovation Center on Forecast and Evaluation of Meteorological Disasters, Nanjing University of Information Science and Technology, Nanjing, Jiangsu, China.*

[3.] *Research Center for Environmental Changes (RCEC), Academia Sinica, Taipei, Taiwan, R.O.C.*

*Corresponded to Yan-Lin Zhang (*zhangyanlin@nuist.edu.cn；dryanlinzhang@outlook.com*)*

ABSTRACT

Arsenic (As) has long been recognized as a toxic element of mainly anthropogenic origins, having adverse effects on human health. However, there is insufficient understanding regarding As released into atmosphere from biomass burning (BB). To this end, daily airborne As concentrations in total particulate matter (TSP) were determined at Mount Hehuan (24.16°N, 121.29°E, 3001 m a.s.l.), Taiwan from September 2011 to September 2012. During the sampling period, As concentrations varied from 0.02 to 5.9 ng m^{-3}, with a mean value of 0.5 ± 1.0 ng m^{-3}. Significant seasonal variations of As were found over the subtropical free troposphere, and higher As concentrations were observed in the South (S) and Southeast (SE)

Asian BB seasons (from January to May). Principal component analysis (PCA) results showed that BB activities seemed to be a major source for As during the S and SE Asian BB periods, which was very distinct from the source of coal-fired power plant during the periods between July and December. Based on backward trajectory analyses and WRF-Chem model simulations, we found the high As concentrations during the BB periods were attributed to the biomass burning activities over S Asia where ground water, soil and crops are severely contaminated by arsenic. A good correlation (r = 0.73 p < .05) between As and potassium ion (K^+, a chemical tracer of BB activities) in S Asian BB events also supported this hypothesis. During the S Asian BB events, the high As/Pb ratios (> 0.2) were also observed, indicating that burning crops contaminated by lead arsenate might be a crucial candidate for high As concentrations at Mount Hehuan. Nevertheless, the net influence of S Asian BB activities on airborne As concentrations has been estimated by comparing the differences of As concentrations between BB and non-BB days. On average, the difference of As concentrations on the BB and non-BB days was 1.0 ng m^{-3}, which accounted 63 % for the average As concentration on BB days. Moreover, a ratio of ΔAs/ΔCO (~0.00001) in the S Asian BB events was obtained. Using this value, arsenic emissions from S Asian BB activities were estimated to be 0.17 tons yr^{-1}, resulting in high airborne As concentrations over the subtropical free troposphere, and impacted As cycles on a regional scale in the S and SE BB seasons.

Key words: Arsenic; Subtropical free troposphere; South Asia; Biomass burning; As/Pb ratios.

1. Introduction

Arsenic (As), categorized into carcinogenic species by International Agency for Research on Cancer, is a toxic element and even in trace concentration may exert hazard to human health. It is also the most highly accumulated trace metal in the human food chain. Consequently, As has been an environmental concern in terms of its emissions, cycling and health effects (Nriagu, 1989; Bissen and Frimmel, 2003; Wai et al., 2016). Atmospheric arsenic is released from both natural and anthropogenic sources with a total annually global emission of nearly 31 Gg (Nriagu, 1989; Wai et al., 2016; Walsh et al., 1979). The quantity of As emissions derived from anthropogenic sources is about 1.6 times higher than that of natural origins (Nriagu, 1989). Arsenic released from volcano is the predominant source of natural emissions, followed by wind-erosion soil particles as well as biogenic emissions (Nriagu, 1989). For anthropogenic sources, metal smelting and coal combustion release quantities of arsenic into atmosphere (Brimblecombe, 1979; Mandal and Suzuki, 2002), and thereby are considered to be major origins for airborne arsenic. Besides, biomass burning (BB) for waste timber treated by As-contained insecticides and crops contaminated by pesticide might enhance the emissions of airborne particulate arsenic (Huang et al., 2012; Niyobuhungiro and Blottnitz, 2013). However, the influence of BB activities on As concentrations over the free troposphere is well not understood.

Biomass burning activity emits large amounts of air pollutants into atmosphere (e.g. carbon monoxide (CO), carbon dioxide (CO_2), nitrogen oxides (NOx), volatile organic compounds (VOCs) and particulate matters (PM)) (Streets et al., 2003；Tang et al., 2003). It impacts not only on local but also on regional air quality, atmospheric chemistry, biogeochemical process and hydrological cycle along with climate (Crutzen and Andreae, 1990; Ramanathan, 2001; Pochanart et al., 2003; Tang et al., 2003; Kondo et al., 2004). Southeast (SE) and South (S) Asia are active biomass

burning regions in the world and BB activities in these continents are mostly caused by deforestation and agricultural activities. Indonesia, India, Myanmar and Cambodia are major countries of BB activities (Chang and Song, 2010; van der Werf et al., 2017). Among these burned areas, BB activities in India are mainly caused by burning of crop residues (~61% of total burning) and frequently occur from January to May and usually maximizes in springtime (Nriagu, 1989; Pochanart et al., 2003). Most BB smokes are emitted within boundary layer. After burning, some BB plumes would uplift from ground level to free troposphere (2-6 km), transporting to the Pacific region by prevailing westerly wind, and then impact on atmospheric chemistry in the downwind regions (Kondo et al., 2004; Lin et al., 2009; Val Martin et al., 2010).

Over the past decade, numerous studies have shown that west Bengal of India and Bangladesh are extremely As-contaminated areas in South Asia (Robert et al., 2010; Neumann et al., 2010; Burgess et al., 2010). The extremely As-contaminated ground water in these areas is used for both drinking and irrigation. Thus, accumulation of As would be found in rice roots and rice plants along with crop soils (Norra et al., 2005). While burning As-contaminated plants, As would be expected to attach within BB-originated aerosols and probably condense on the existing aerosols, and transport to the downwind site, enhancing the atmospheric As concentrations in aerosol phase (Huang et al., 2012).

Mountain-top site, which is generally situated far away from direct influence of local anthropogenic emissions, is very sparsely in the Northern Hemisphere. Due to the high elevation, mountain-top site is useful to monitor long-range transported air pollutions (Weiss-Penizas et al., 2007; Lin et al., 2013). From September 2011 to September 2012, the continuous measurements of total suspended particulate (TSP, dynamic diameter less than 100 μm), ozone and carbon monoxide were carried out at

Mountain Hehuan in Taiwan, with the aim to better understand the behaviors of air pollutants transported horizontally from Asian continent and intruded vertically from high-troposphere/low-stratosphere over the subtropical region. Chemical compositions of TSP samples, including water-soluble ions and elements, were analyzed. In this paper, we present the As concentrations and its seasonality at Mount Hehuan. The potentially regional sources of high As concentrations are also examined by backward trajectory analyses and WRF-Chem model simulations. Finally, the net influence of SE and S Asian BB activities on airborne As over the subtropical free troposphere is assessed. To our best knowledge, this is the first paper to report regionally transported arsenic accompanying with BB plumes and enhancements in airborne As concentrations over the subtropical free troposphere.

2. Method

2.1 Aerosol sampling

Daily TSP samples were collected at Mount Hehuan site, Taiwan (24.16 °N, 121.29 °E, 3001 m a.s.l., see in Figure 1) from September 2011 to September 2012. The sampling station is located in a pristine environment and its vicinity is generally higher than 2900 m, and thereby the monitoring site can be considered as representative of the free troposphere over the subtropical Pacific region (Lin et al., 2013). A high-volume TSP sampler (TISCH, Model TE-5170D), operated at a flow rate of approximately 1.13 m^3 min^{-1}, was used to collect aerosol samples. Whatman®41 cellulose filters (8” × 10”) were used as filtration substrates. After sampling, each filter was folded and stored in a separate plastic bag that was then stored in a polypropylene container, frozen immediately, and returned to the laboratory for further chemical analysis. Carbon monoxide, a tracer for tracking

anthropogenic plumes, was monitored by a nondispersive infrared spectrometer (Horiba model APMA-370). The details of the instrument and QA/QC procedure for CO monitoring are described elsewhere (Lin et al., 2013).

2.2 Chemical Analysis

For the purpose of chemical analyses, the sampled filter was subdivided into eight equal pieces after sampling. One piece was subjected to acidic digestion for elemental determination and another one was extracted by Milli-Q water for analyzing water-soluble ions. For acidic digestion, each filter sample was put into an acid-cleaned vessel and digested in a mixed acidic solution (4 mL 60 % HNO_3 + 2 mL 48 % HF) by an ultrahigh throughput microwave digestion system (MARSXpress, CEM Corporation, Matthews, NC, USA). The digestion process was performed in three steps: (1) heating to 170 °C for 8 min and maintaining this temperature for 7 min at 1440 W, (2) heating to 200 °C for 7 min and maintaining this temperature for 15 min at 1600 W, and (3) cooling for 60 min. Subsequently, the vessel was transferred to XpressVap^{TM} accessory sets (CEM Corporation) for the evaporation of the remaining acids until nearly dry. Approximately 2 mL concentrated HNO_3 was added into the vessel and reheated. The resulting solution was then diluted with Milli-Q water to a final volume of 50 mL. After acidic digestion, 31 target elements in TSP samples were analyzed through inductively coupled plasma mass spectrometry (ICP-MS; Elan 6100; Perkin ElmerTM, USA). A multi-element standard, prepared from stock (Merk) composed of 2 % HNO_3 solution, was used for calibration. An internal standard containing indium (10 ng mL^{-1}) was used to correct instrumental drift. To minimize the isobaric interference, the nebulizer gas flow rate was adjusted to 0.7 - 0.9 L min^{-1}. To reduce formation of doubly charged ions and oxides, Ba^{++}/Ba

and CeO/Ce must be lower than the recommended values of 0.01 and 0.02, respectively. Accuracy and precision were assessed by replicate measurements (N=7) of the standard reference material NIST SRM 1648, following the total digestion process. The results showed that the recoveries for most elements fell within 90-110% and the precisions were less than 5 %. Arsenic, a target element, exhibited a recovery of 106 % and a precision of 2 %. For each run, a blank regent and three filter membrane blanks were subjected to the same procedure as that for the aerosol samples. The method detection limits (MDLs) were 0.01 ng m^{-3} for both As and Pb.

Another half of the filter sample was extracted with 20 mL Milli-Q water (18.2 Ω) by using ultra-sonic apparatus for 1h. The extracted solution was subsequently analyzed for water-soluble ions, including Na^+, NH_4^+, K^+, Mg^{2+}, Ca^{2+}, Cl^-, NO_3^-, and SO_4^{2-}, by ion chromatography (Dionex ICS-90 for cations and ICS-1500 for anions) equipped with a conductivity detector (ASRS-ULTRA). A QA/QC program including calibration, recovery and precision test along with MDLs for all ions was conducted during the analyzed processes. A multi-ion solution (Merck) was used for calibration of IC instrument and seven-point calibration curves were made for each batch of samples. One laboratory blank was taken for each batch analysis and MDL was calculated as 3 times standard deviation of the values of 7 blanks. The average recoveries for all species were in the range of 91-105 %; the precisions for all species were less than 5 %.

2.3 Principal component analysis

Principal component analysis (PCA), as a technique which attempts to explain the statistical variance in a given dataset in terms of a minimum number of significant components, has been widely employed to identify potential sources for airborne

particulate matters observed at a receptor site (Vina et al., 2006; Venter et al., 2017). To compute PCA model, the first step was to transform the chemical data into normalized form as:

$$Z_{ij} = \frac{C_{ij} - \mu_j}{\sigma_j} \quad (1)$$

where Z_{ij} is the normalized value of the species j in i sample. Cij is the concentration of species j in sample i; μ_j and σ_j are the mean concentration and standard deviation for species j. The PCA model was then expressed as:

$$Z_{ij} = \sum_{k=1}^{n} g_{ik}\, h_{kj} \quad (2)$$

where k=1, …, n represents the different sources, and g_{ik} and h_{kj} are the factor loading and factor score, respectively. Associated with each component is an eigenvalue; only principal components with eigenvalue greater than 1.0 were selected to identify aerosol sources. The software of SPSS (IBM statistics 19) was performed for PCA analysis.

2.4 Backward trajectory analysis

To identify potential sources of airborne arsenic at Mount Hehuan, five-day backward trajectories were computed by the Hybrid Single-Particle Lagrangian Integrated Trajectory (HYSPLIT) model developed by the USA NOAA Air Resources Laboratory (Draxler and Hess, 1998). The meteorological data for the trajectory model was the GDAS (Global Data Assimilation System), which were processed by the NCEP with a 6-h time resolution, about 190 km horizontal resolution, and 23 vertical levels. In this work, five-day backward trajectories arriving at 3000 m a.s.l. were computed at 12:00 LT (local time) once every day with a time step of 6 hours.

Four additional trajectories were generated of which starting locations were changed ± 0.5° from the actual sampling site to reduce the uncertainty of the trajectory analysis. During the sampling period, a total of 1865 backward trajectories were computed. According the originated regions of air parcels, we divided the trajectories into five groups, namely, Northern China (NC), Pacific Ocean (PO), South Sea (SS), Southeast Asia (SEA) and South Asia (SA).

Figure 1 shows the pathways of five different air clusters at Mount Hehuan. The frequency of SA was 33%, which was the predominant air clusters, followed by PO (24%), SS (18%), SEA (18%) and NC (7%). In the NC group, the air mass originated mainly from Northern China, where heavily polluted air is contaminated by industrial emissions, moving to the south areas slowly and then arrived at the receptor site. The NC air cluster was predominately found in March, August and September with a frequency of > 16 % (shown in Figure 2). In case of PO, the air parcel generally came from Western Pacific Ocean, spending much time in marine atmosphere before arriving at Taiwan. This air cluster was most predominately found from July to September with a frequency of > 48 %. High frequency (> 20 %) of PO cluster was also surprisingly found in October and November. For SS air cluster, the air parcel was regularly from South Sea, crossing the marine areas or Luzon Islands, and then arrived at Mount Hehuan. This air group accounted for 18 % with a high frequency in June, July and November. For SEA group, the air mass typically came from Indo-China Peninsula, occasionally passing across polluted Southern China, like Sichuan Basin and Pearl River Delta (PRD) region, before reaching Taiwan. The SEA air group was profoundly occurred from March to June with the frequency exceeding 30 %. Finally, the air parcel of the SA cluster was mainly from Middle East and Indian Subcontinent, passing over northern parts of Myanmar, Thailand, Laos and

Vietnam along with PRD region, and then descended to Mount Hehuan. The SA group was frequently found during the sampling periods, except for July to September. The air masses of NC, SEA and SA groups were associated with continental origins as they spent much time in Asia continent before arriving at Mount Hehuan. The continental air masses were mostly prevailed from mid-autumn to late spring (see in Figure 2). On the contrary, PO and SS air clusters were grouped into marine air parcels and were profoundly found from June to September. Nevertheless, the air parcels from NC, SEA and SA groups would be anticipated picking up polluted air and transporting to Mount Hehuan compared with PO and SS air clusters that spent much time in marine atmosphere.

2.5 WRF-Chem model

To simulate long-range BB plumes transported to Mount Hehuan, the WRF model coupled with chemistry module (WRF-Chem; Ver. 3.2.1) was employed. Previously, this model has been successfully simulated and identified the biomass burning transportation from SE and S Asia (Chi et al. 2010; Lin et al. 2009; 2014). In this study, a tracer module in WRF-Chem developed by Lin et al (2009) was employed to identify the transport. The tracers were assigned to the fire locations derived from MODIS satellite data over the study domain. They were placed at the first level above the surface at each fire location with a concentration of 1 unit per day. The dry and wet deposition functions are considered in the model. The meteorological initial and boundary conditions for WRF-Chem were acquired from NCEP-FNL Global Forecast System (GFS) 0.5° × 0.5° analysis data sets (35 vertical levels). The Mellor Yamada Janijc (MYJ) planetary boundary layer scheme was selected in this study. The horizontal resolution for our BB simulations was 27 km. To assure the

meteorological fields were well simulated, the four-dimensional data assimilation (FDDA) scheme was activated based on the NCEP-GFS analysis data.

2.6 MODIS fire spots

The fire spots from BB activities were extracted by the Moderate Resolution Image Spectroradiometers (MODIS) on board NASA's polar-orbit Aqua and Terra satellites. MODIS fire detection algorithm employs infrared spectrum channels of 4 μm and 11 μm (Kaufman et al., 1998). The 1-km Level-2 active fire products, abbreviating MOD14 and MYD14, provide the detection time, coordinates, confidence, bright temperature for each fire pixels (Giglio, 2013). Details of the fire detection algorithm was discussed by Giglio et al. (2003). In this work, MODIS Level- 2 fire spots observed within a domain (65°E~135°E and 5°N ~ 40 °N) from September 2011 to September 2012 were obtained. We used the datasets to analyze the monthly distributions of BB activities over the SE and S Asian continent.

3. Results and discussion

3.1 Overview of Airborne Particulate As

A total of 302 daily TSP samples were collected at Mount Hehuan during the sampling period. Each TSP sample has been determined the concentrations of water-soluble ions and elements by IC and ICP-MS, respectively. Because the net mass of each collected aerosol sample was not measured, the abundance of each species relevant to TSP mass cannot not be obtained. Figure 3 displays the average concentrations of ionic species together with metallic elements in TSP samples. All the concentrations are presented under prevailing conditions. Without determination of carbon contents, sulfate was the most predominant species in airborne TSP samples

with a mean concentration of 4.1 μg m^{-3}, followed by nitrate (2.0 μg m^{-3}), ammonium (1.7 μg m^{-3}) and chloride (0.23 μg m^{-3}). Aluminum (Al), a typical geological material, exhibited a mean concentration of 184 ng m^{-3}, which was the predominant elements. In addition to K, Ca and Fe (up to 100 ng m^{-3}) were also major metals, followed by Na, Mg, Cu, Ti, Zn and P (10 to 100 ng m^{-3}), and then followed by Pb, Mn, Ba and Sr (1 to 10 ng m^{-3}). The rest metals had concentrations of < 1 ng m^{-3} over the free troposphere. As expected, high concentrations for all species were found for the continental air clusters, including NC, SEA and SA air groups (see in Table S1). In particular, the SA air parcel picked up heavily polluted air to the receptor site since the concentrations of secondary inorganic aerosols (SIA, including SO_4^{2-}, NO_3^- and NH_4^+) and crustal materials (Al, Fe, Ca, Na, K, Mg and Sr) were significantly higher than those of other continental air clusters. Although the reason was not well understood, it might be attributed to the different emission sources the air passed and atmospheric processes during their long-range transport.

Arsenic, a target element in this study, exhibited a daily concentration from 0.02 to 5.9 ng m^{-3} with a mean value of 0.5 ± 1.0 ng m^{-3} (Figure S1). As expected, arsenic concentrations in the continental air groups, such as SA, NC and SEA, were much higher than those in the marine air categories (Figure 1 and Table S1). The As concentrations (~0.1 ng m^{-3}) in PO and SS air groups were in agreement with that of Mauna Loa, Hawaii (Zieman et al., 1995), indicating that the low As value can be considered as a background value in the subtropical free troposphere (Zieman et al., 1995). A large standard deviation suggested that As concentration at this mountainous site had a large day-to-day variation. Some As peaks were found with enhancements of both CO and potassium ion (K^+), especially between January and May, indicating BB origins.

Figure 4a shows monthly variations of 75th, 50th and 25th percentile values of arsenic concentrations observed at Mount Hehuan. As can be seen, the median concentration of arsenic increased from January (0.18 ng m^{-3}), maximizing in May (0.81 ng m^{-3}), and then decreased abruptly through June to December (from 0.05 ng m^{-3} in June to 0.13 ng m^{-3} in August). The seasonality of As was different from those of Al (a tracer of dust) and K^+ (a marker of BB) as shown in Figures 4b and 4c, but was very similar to that of Pb (Figure 4d), suggesting As and Pb might be originated from the similar sources. The seasonal distributions of As at this mountainous site were associated with emission sources, regional circulations and local meteorological conditions. Marine air prevailed from July to November, except October, resulting in lower As concentrations over the subtropical free troposphere. On the contrary, continental air prevailed in the wintertime and springtime, picking up polluted air and transported to the receptor site; as a result, increase of As concentrations was expected. Besides, favorable locally meteorological conditions for dispersion of air pollution might be another reason for the lower As concentrations in the summertime (Lin et al., 2011; 2013).

The 95th percentile value for As concentration is better to understand the distributions of extremely high As events over the free troposphere. Higher 95th percentile values of arsenic were found between February (0.99 ng m^{-3}) and May (1.27 ng m^{-3}) compared to those of other seasons (from 0.09 ng m^{-3} in November to 0.60 ng m^{-3} in September), reflecting more high-As plumes crossed over Mount Hehuan from late-winter to late-spring. Over the subtropical free troposphere, two distinct haze plumes were usually observed from late winter to spring: one is dust storm that originated from East-Asian and non-East Asian continents (Lin et al., 2001; Hsu et al., 2012); another one is BB plume which mainly comes from SE and S Asia

(Lin et al., 2009; 2010). As shown in Figures 4b and 4c, substantially elevated Al and K^+ concentrations were observed in the springtime, especially for 75th percentile values, suggesting that Mount Hehuan was influence by both dust and BB aerosols. Both specific plumes would impact the atmospheric compositions, of course, including airborne As in Pacific region.

3.2 Potential source for As in the BB seasons

As mentioned earlier, high As concentrations were observed during the SE and S Asian BB seasons. In this section, we attempted to investigate the potential sources of high As concentrations at Mount Hehuan. Table 1 lists the PCA results of TSP observed at Mount Hehuan during the SE and S Asian BB seasons and non-BB seasons (from June to December). The results showed that there were three factors of TSP during the BB seasons. PC1 was associated with a mixed source of crustal materials (high loading of Al, Fe, Mg, Ca, Sr, Ti, Mn and Rb along with La, Ce and Nd), SIA (high loadings of SO_4^{2-}, NO_3^- and NH_4^+) and industrial emissions (high loadings of Ni, Mo, Tl, V and Se). In PC2, a high loading was found for K^+ and a moderate loading for CO, indicating BB sources. Interestingly, moderate loadings were also found for As and Pb, suggesting both species might be from BB activities. The PC3 was regarded as sea salt aerosols since the high loadings were found for Na^+ and Cl^-. During the non-BB periods, three factors were also assessed. The PC1 was assigned as a source related to crustal materials with high loadings of Al, Fe, Mg, Ca, Sr, Ti, Mn, Rb, La, Ce and Nd. In terms of PC2, high loadings of Tl, As and Se were found, suggesting industrial emissions. In particular, highly positive loadings were found for As and Se, indicating that As at Mount Hehuan during the non-BB seasons was mainly attributed to coal-fired power plant which was very different from the

result during the periods from January to May. The PC3 exhibited high loadings of SO_4^{2-}, NO_3^- and NH_4^+ together with Na^+ and Cl^-, reflecting SIA and sea salt aerosols.

Figure 5 shows the scattered plots of As against K^+, Al and Pb in different arsenic concentration bins. We found that As correlated well with K^+ ($r = 0.78$, $p < .05$ for the 95th percentile value of As) when severely high As events occurred, suggesting BB origins. Oppositely, arsenic correlated poorly with Al (r ranged from 0.05 to 0.42) in all As concentration bins, indicating that wind-erosion soil was not a major source for airborne As at the sampling site. However, significantly positive correlations were observed between As and Pb within 75th percentile As values, reflecting that airborne As and Pb were from the similar sources in the high arsenic events.

As discussed above, BB activities may be an important regionally source for high As concentrations over the subtropical free troposphere, especially during the SE and S Asian BB seasons; consequently, we tried to prove the hypothesis using backward trajectory analyses and MODIS fires observations together with WRF-Chem model simulated results. Figure S2 shows the seasonality of fire spots over SE and S Asia observed by MODIS from 2011 September to 2012 September. In SE Asia, the BB activities showed strong seasonal variations with a gradual increase from January to March, when it reached a peak. It then decreased substantially from late spring to a minimum in summer. In South Asia, the total annual counts of fire spots were approximately 20 % of that in SE Asia. Similar seasonality was found with intensive fire spots in the springtime and maximum in May. The fire spots then decreased during summer to mid-winter and minimized in July. However, the total fire spots (SE Asia plus S Asia) maximized in March. This might explain why particulate K^+ and CO concentrations at Mount Hehuan were highest in March.

For convenience, prior to further analysis we arbitrarily chose a K^+ concentration of 109 ng m^{-3} (the 75th percentile value of potassium ion) as a criterion value for identifying the suspected BB events. A second criterion (CO concentration up to 160 ppb) was also added for selection of the BB plume. Ultimately, a total of forty-nine suspected BB TSP samples were identified during the entirely sampling period. Figure 6 shows time series of daily concentrations of As, K^+ and CO observed at Mount Hehuan from January to May, 2012 when intensive BB activities were occurred over SE and S Asia. The air clusters are also shown in this figure for helping to identify the air origins. As can be seen, several As spikes coincided with increasing CO and K^+ (e.g. Feb. 19, Mar. 30, Mar. 31, Apr. 3, May 5 and 7 etc.), implying BB origins. Backward trajectory showed that the air parcels for the high arsenic events originated mainly from S Asia (see in Figure S3a). A high arsenic plume passed over Mount Hehuan with As concentration increasing from 1.2 ng m^{-3} on 25 March to 5.3 ng m^{-3} on 3 April though low As concentration was found on 2 April. Figure S4a illustrates the five-day backward trajectories starting at Mount Hehuan during this period. The result showed the air parcels mainly passed over northern India, Nepal, Bangladesh and Southeast China before arriving at Taiwan. Figure 7a plots the distributions of MODIS fires from March 25 to April 3, and WRF-Chem model result at an altitude of 700 hPa on April 3 when the high daily As concentration (5.3 ng m^{-3}) was observed. As seen, extensive fire spots were observed over Indian Subcontinent from March 25 to April 2. In this case, the tracers were assigned to the fire locations derived from MODIS satellite data over Indian Subcontinent ranging from 5 to 38 °N and 65 to 90 °E and they were placed at the surface level above the surface at each fire location with a concentration of a unit per day. The WRF-Chem model result showed that the significant BB plume originated over burned areas, transporting to east direction, and

passed over Mount Hehuan, resulting in increased concentrations not only for K^+ and CO, but also for arsenic. As shown in Figure 8a, during the BB events over the S Asian continent, arsenic correlated well with K^+ (r =0.73, p < .05). On the contrary, the correlation coefficient between As and K^+ in the non-BB events was 0.53 (p > .05). This supported our argument, that is, airborne arsenic at Mount Hehuan was attributed to BB activities over S Asia.

Some BB plumes were observed at Mount Hehuan, but the As concentrations were not elevated. For example, a suspected BB plume was found from March 8 to 15 since K^+ and CO concentrations increased concurrently. Based on backward trajectory analysis, the air parcels during this BB event were mainly from SE Asia, passing over southeast China, and then arrived at Mount Hehuan (Figure S4b). Because backward trajectories were mainly from Indo-China Peninsula, the tracers were then placed at the surface level above the surface at each fire location in Indo-China Peninsula ranging from 5 to 30 °N and 90 to 110 °E. The WRF-Chem model showed that the significant tracer concentration laid in northeast-southwest belt and covered Taiwan on March 15 (as shown in Figure 7b). Nonetheless, the As did not rise, but kept at the low levels of 0.2 ng m^{-3}. Another similar case was also found in the end of February (Feb. 25 to 28). The backward trajectories also showed that the air masses were mainly from Indo-China Peninsula (see in Figure S3b). Unlike BB events over S Asia, arsenic correlated weakly with K^+ (r = 0.4, p >.05, Figure 8b) in the BB events from SE Asia, as well as that in the maritime air groups (Figure8c). These findings suggested that some specific sources might release numerous arsenic into atmosphere during BB activities over S Asia, but not over Indo-China Peninsula.

Wind-erosion soil particles are one of important sources for airborne arsenic. According to the investigation by Nriagu (1989), arsenic derived from wind-erosion

426 dust was 2.1 Gg yr^{-1}, accounting 18% for natural As emissions. Figures S4a – S4c
427 show the scattered plots of As against Al in all air groups during the S and SE Asian
428 BB periods. Poor correlations were found between As and Al in the various air groups,
429 except for the SS air category (r = 0.88, p <.05), indicating that wind-erosion soil was
430 not a major source for As over the free troposphere. Interestingly, a good correlation
431 of As and Al was found in the SS air group. The marine air parcels, which spent a
432 long time in the clean marine atmosphere, are subjected to dilution which can affect
433 the air pollution (Lin et al., 2011), probably resulting in similar behaviors of As and
434 Al.

435 Recently, numerous studies pointed out S Asia, especially in west Bengal of
436 India and Bangladesh, are extremely As-contaminated areas (Burgess et al., 2010;
437 Neumann et al., 2010; Roberts et al., 2010;). In these regions, highly As-contaminated
438 ground water, typically caused by geological process, is not only used for drinking
439 water, but is also used for irrigation of crops. Accumulation of arsenic has been found
440 in rice roots and rice plants along with crop soils (Norra et al., 2005). After burning,
441 the As might be released from these crops into atmosphere, and transported easterly to
442 Pacific regions with BB plumes. On the other hand, uses of pesticide as an insecticide
443 for cotton, paddy and wheat in India and Bangladesh might be another reason for As
444 contamination in crops (Aktar et al., 2009). Lead arsenate (LA, $[Pb_5OH(AsO_4)_3]$;
445 As/Pb~0.22) was the most extensively used as the arsenical insecticides in the world.
446 It was used as an insecticide for gypsy moths invading hardwood forests in 1892. LA
447 can be adhered to the surfaces of plants. Although LA was officially banned as
448 insecticide in 1990's in many developed countries, but has not been banned in India
449 nowadays. Figures 9a and 9b show the scattered plots of As against Pb in TSP
450 samples for various air groups during the S and SE Asian BB season. The higher As

concentrations were generally found in the SA air category. In case of SA air group, the average As concentration in the BB events were 1.6±1.4 ng m^{-3}, exceeding that (0.6±0.7 ng m^{-3}) in non-BB events by a factor of 2.7 ($p < .05$), suggesting a special arsenic emission source over S Asian continent during the BB season. In some cases, low As concentrations were also found when the BB plumes transported from S Asia. The reason has not been clearly understood, but might be explained by a mixed source of the BB plume with other emissions during the air transportation. In terms of SEA group, no substantial discrepancy of As concentrations was found during BB and non-BB periods, indicating that BB over Indo-China Peninsula was unable to enhance As concentrations over the subtropical free troposphere.

During the S and SE Asian BB period, good correlations between As and Pb (ranging from 0.84 for SA-BB to 0.96 for NC, see in Figure 9) were found in various air groups; hence, a ratio of As/Pb might be given us an insight to trace the specifically regional arsenic emissions in SA air group when BB activity occurred. During the SA-BB plumes, the average As/Pb ratio was 0.18 (see in Figure 9a), which was much higher than the average value (0.11) of non-BB (SA-non-BB) events along with those (ranging from 0.08 to 0.1) of other air categories (see in Figures 9b and9c), implying a special source for As during the BB events over S Asia. Some data sets of SA-BB groups showed low As/Pb ratios, probably reflecting mixed air of BB plumes and other emission sources transported to the subtropical free troposphere.

Wind-erosion soil particles and metal smelting (lead smelting) along with coal combustion industries are major natural and anthropogenic sources of airborne As, respectively. In Northern India, As/Pb ratio in natural soil, paved road and unpaved road dust varied from 0.02 to 0.13 while low As/Pb ratios were found in lead smelting (0.002), coal combustion in stoves (0.0016) and coal fire power plants (0.0026) (Patil

et al., 2013). Our As/Pb ratios in the SA-BB events were much higher, suggesting that wind-erosion dust, lead smelting and coal combustion seemed not to be major sources. In particular, the As/Pb ratio was normally higher than 0.20 when severely high As concentrations were observed. This ratio was in line with that of LA (~0.22), suggesting that burning crops contaminated by LA in S Asia could be a crucial candidate for extremely high As concentrations at Mount Hehuan during the BB periods.

3.1 Impact of Biomass Burning

The differences of As concentrations between the BB and non-BB days could be roughly considered as the net influence of BB activities on the airborne As concentrations over the subtropical free troposphere (Lin et al., 2010; 2013). Table 2 lists the differences of As, Pb, K^+ and CO concentrations of BB and non-BB samples in SA and SEA air groups in the S and SE Asian BB seasons. For SA air cluster, all species increased apparently in the BB events. On average, the As concentrations in the BB and non-BB events were 1.6 and 0.6 ng m^{-3}, respectively. The difference (1.0 ng m^{-3}) accounted 63 % for the average As concentration on the BB days. This indicated that S Asian BB activities played an important source for high As concentrations. On the contrary, the differences of concentrations in K^+ and CO were observed in the BB and non-BB events for SEA air clusters, but not found for As and Pb. Again, this suggested that BB activities from SE Asia would not release enormous arsenic into atmosphere and transport to the subtropical free troposphere by westerly belt.

From Table 2, we identified ΔK^+, ΔCO and ΔAs as the differences of concentrations in K^+, As and CO between BB and non-BB days in S and SEA air

clusters during the BB seasons. Here, we also converted the units of daily K^+ and As concentrations from ng m^{-3} to ppb based on the ambient temperature and molecular weight of K^+ and As; then, we can obtain the ratios of $\Delta K^+/\Delta CO$ and $\Delta As/\Delta CO$ without units. The parameters are useful to estimate the K^+ or As emissions from BB activities over S and SE Asia. As listed in Table 2, the BB air masses emitted from the S and SE Asian continents contained $\Delta K^+/\Delta CO$ ratios of 0.0043 and 0.0018, respectively. Each value was in the same order of magnitude of that estimated by Tang et al. (2003) who claimed the BB events emitted from SE Asia had a $\Delta K^+/\Delta CO$ ratio of 0.0038. Besides, a ratio of $\Delta As/\Delta CO$ in the S Asian BB events was estimated to be 0.00001, which was one order of magnitude higher than that ($\Delta As/\Delta CO$~0.000001) of SE Asian BB events, indicating that much more As released into atmosphere from the S Asian continent. According to the emission inventory, the annual CO emission rate from biomass burning over S Asia was nearly 17 Gg y^{r-1} (Stress et al., 2003), we then roughly estimated that approximately 0.17 tons yr^{-1} of arsenic was released into atmosphere due to S Asian BB activities, resulting in enhancements of As concentrations over the subtropical free troposphere.

4. Conclusion

Daily TSP samples were collected at Mount Hehuan from September 2011 to September 2012, in order to investigate the behaviors of long-range transported particulate matters and their impact on atmospheric chemistry over the subtropical free troposphere. Arsenic, a target metal in TSP samples, were determined by ICP-MS. The results showed the daily As concentrations varied from 0.02 to 5.9 ng m^{-3} with a mean value of 0.5 ± 1.0 ng m^{-3}. Some high As concentrations coincided with concurrent enhancements of K^+ and CO. PCA results indicated that high As

concentrations were contributed by BB emissions during the S and SE Asian BB seasons. Backward trajectory and WRF-Chem model results suggested that the high As plumes originated mainly from S Asia. The ratio of As/Pb (> 0.2) in high As events elucidated burning crops contaminated by lead arsenate might be an important source of high As concentrations at Mount Hehuan. Furthermore, biomass burning over S Asia produced an As/CO ratio of 0.00001 and released approximately 0.17 tons of As into atmosphere every year, causing increase in As concentrations over the subtropical free troposphere.

Asian continent is well known a big source of airborne As in North Pacific region. Previously, high As concentrations over free troposphere in Northern Pacific region have been considered as contributions of industrial emissions (Perry et al., 1990; Wai et al., 2016). From our study, we proposed a new concept for a potential source of high As over the subtropical free troposphere, that is, BB activities over S Asia might be an important source of airborne arsenic. In this study, arsenic emissions from S Asian BB activities was estimated to be 0.17 ton yr^{-1}. Compared to the globally anthropogenic arsenic emissions (~18.8 Gg yr^{-1}, Nriagu and Pacyan, 1988), arsenic released from the S Asian BB activities seemed to be neglected. Indeed, As concentrations at the receptor site did increase significantly when the BB plumes transported from S Asia to Mount Hehuan. Consequently, we concluded that BB activities over S Asia could certainly impact arsenic cycles on a regional scale that has never been considered in previous studies.

Acknowledgements

This study was financially supported by the Natural Scientific Foundation of China (No. 91643109), the National Key Research and Development Program of

China (No. 2017YFC0210101), and the Ministry of Science and Technology of R.O.C. (No. MOST 104-2111-M-001-009-MY2).

Reference

Aktar, M. W., Sengupta, D., and Chowdhury, A.: Impact of pesticides use in agriculture: their benefits and hazards. Interdiscip. Toxicol., 2, 1-12, doi:10.2478/v10102-009-0001-7, 2009.

Bissen, M., and Frimmel, F.H.: A review. Part I: occurrence, toxicity, speciation, mobility. Acta Hydroch. Hydrob., 31, 9-18, doi:10.1002/aheh.200390025, 2003.

Brimblecombe, P.: Atmospheric arsenic. Nature, 280, 104-105, doi:10.1038/280104a0, 1979.

Burgess, W. G., Hoque, M. A., Michael, H. A., Voss, C. I., Breit, G. N., and Ahmed, K. M.: Vulnerability of deep groundwater in the Bengal Aquifer System to contamination by arsenic. Nat. Geosci., 3, 83-87, doi:10.1038/NEGO750, 2010.

Chang, D., and Song, Y.: Estimates of biomass burning emissions in tropical Asia based on satellite-derived data. Atmos. Chem. Phys., 10, 2335-2351, doi: 10.5194/acp-10-2335-2010, 2010.

Chi, K. H., Lin, C.-Y., Ou-Yang, C.-F., Wang, J.-L., Lin, N.-H., Sheu, G.-R., and Lee, C.-T.: PCDD/F measurement at a high-altitude station in central Taiwan: evaluation of long-range transport of PCCD/Fs during the Southeast Asia biomass burning event. Environ. Sci. Technol., 44, 2954-2960, doi:10.1021/es1000984.

Crutzen, P. J., and Andreae, M. O.: Biomass burning in the Tropics-impact on atmospheric chemistry and biogeochemical cycles. Science, 250, 1667-1678, doi: 10.1126/science.250.4988.1669, 1990.

Draxler, R. R., and Hess, G. D.: An overview of the HYSPLIT_4 modeling system for

trajectories, dispersion and deposition. Aust. Meteor. Mag., 47, 295-308, 1998.

Giglio, L., Descloitres, J., Justice, C. O., Kaufman, Y. J., 2003. An enhanced contextual fire detection algorithm for MODIS. Remote Sens. Environ., 87, 273-282, doi:10.1016/S0034-4257(03)00184-6.

Hsu, S.-C., Hus, C.-A., Lin, C.-Y., Chen, W.-N., Mahowald, N. M., Liu, S.-C., Chou, C. C. K., Liang, M.-C., Tsai, C.-J., Lin, F.-J., Chen, J.-P., and Huang, Y.-T.: Dust transport from non-East Asian sources to the North Pacific. Geophys. Res. Lett., 39, L12804, doi:10.1029/2012GL150962, 2012.

Huang, K., Zhuang, G., Lin, Y., Fu, J. S., Wang, Q., Liu, T., Zhang, R., Jiang, Y., Deng, C., Fu, Q., Hsu, N. C., and Cao, B.: Typical types and formation mechanisms of haze in an Eastern Asia megacity, Shanghai. Atmos. Chem. Phys., 12, 105-124, 10.5194/acp-12-105-2012, 2012.

Kaufman, Y. J., Justice, C. O., Flynn, L. P., Kendall, J. P., Prins, E. M., Giglio, L., Ward, D. E., Menzel, W. P., Setzer, A. W., Potential global fire monitoring from EOS-MODIS. J. Geophys. Res.: Atmos., 32215-32238, doi: 10.1029/98JD01644, 1998.

Kondo, Y., Morino, Y., Takegawa, N., Koike, M., Kita, K., Miyazaki, Y., Sachse, G. W., Vay, S. A., Avery, M. A., Flocke, F., Weinheimer, A. J., Eisele, F. L., Eondlo, M. A., Weber, R. J., Singh, H. B., Chen, G., Crafword, J., Blake, D. R., Fuelberg, H. E., Clarke, A. D., Talbot, R. W., Sandholm, S. T., Browell, E. V., Streets, D. G., and Liely, B.: Impacts of biomass burning in Southeast Asia on ozone and reactive nitrogen over the western Pacific in spring. J. Geophys. Res. Atmos., 109, D15, doi:10.1029/2003JD004203, 2004.

Lin, C.-Y., Hsu, H.-m., Lee, Y. H., Kuo, C. H., Sheng, Y.-F., and Chu, D. A.: A new transport mechanism of biomass burning from Indochina as identified by

modeling studies. Atmos. Chem. Phys., 9, 7901-7911, doi:10.5194/acp-9-7901-2009, 2009

Lin, C.-Y., Zhao, C., Liu, X., Lin, N.-H., and Chen, W.-N.: Modelling of long-range transported of Southeast Asia biomass-burning aerosols to Taiwan an their radiative forcings over East Asia. Tellus B, 66, 1, doi:10.3402/tellusb.v66.23733, 2014.

Lin, T.-H.: Long-range transport of yellow sand to Taiwan in spring 2000: observed evidence and simulation. Atmos. Environ., 35, 5873-5882, doi:10.1016/S1352-2310(01)00392-2, 2001.

Lin, Y. C., Lin, C. Y., and Hsu, W. T.: Observations of carbon monoxide mixing ratios at a mountain site in central Taiwan during the Asian biomass burning season. Atmos. Res., 95, 270-278, doi:10.1016/j.atmosres.2009.10.006, 2010.

Lin, Y. C., Lin, C. Y., Lin, P. H., Engling, G., Lan, Y.-Y., Kuo, T.-H., Hsu, W. T., and Ting, C.-J.: Observations of ozone and carbon monoxide at Mei-Feng mountain site (2269 m a.s.l.) in central Taiwan: seasonal variations and influence of Asian continental outflow. Sci. Total Environ., 15, 3033-3042, doi:10.1016/j.scitotenv.2011.04.023, 2011.

Lin, Y. C., Lin, C. Y., Lin, P. H., Engling, G., Lin, Y. C., Lan, Y. Y., Chang, C. W. J., Kuo, T. H., Hsu, W. T., and Ting, C. C.: Influence of Southeast Asian biomass burning on ozone and carbon monoxide over subtropical Taiwan. Atmos. Environ., 64, 358-365, doi:10.1016/j.atmosenv.2012.09.050, 2013.

Lin, Y.-C.; Huh, C.-A.; Hsu, S.-C.; Lin, C.-Y.; Liang, M.-C., and Lin, P.-H.: Stratospheric influence on the concentration and seasonal cycle of lower tropospheric ozone: observation at Mount Hehuan, Taiwan. J. Geophys. Res. Atmos., 119, 3527-3536, doi:10.1002/2013JD020736, 2014.

626 Mandal, B. K., and Suzuki, K. T.: Arsenic round the world: a review. Talanta, 58,
627 201-235; doi:10.1016/S00399140(02)00268-0, 2002.
628 Neumann, R. B., Ashfague, N., Badruzzaman, A. B. M., Ali, M. A., Shoemaker, J. K.,
629 and Harvey, C. F.: Anthropogenic influences on groundwater arsenic
630 concentrations in Bangladesh. Nat. Geosci., 3, 46-52, doi:10.1038nego685, 2010.
631 Niyobuhungiro, R.V., and Blottnitz, H.v.: Investigation of arsenic airborne in
632 particulate matter around caterers' wood fires in Cape Town region. Aerosol Air
633 Qual. Res., 13, 219-224, doi:10.4029/aaqr.2012,06.0148, 2013.
634 Norra, S., Berner, E. A., Agarwala, P., Wagner, E., Chandrasekharam, D., and Stüben,
635 D.: Impact of irrigation with As rich groundwater on soil and crops: a
636 geochemical study in West Bengal Delta Plain, India. Appl. Geochem., 20,
637 1890-1906, doi:10.1016/j.apgeochem.2005.04.019, 2005.
638 Nriagu, J. O., and Pacyna, J. M.: Quantitative assessment of worldwide contamination
639 of air, water and soils by trace metals. Nature, 333, 134-139,
640 doi:10.1038/333134a0, 1988.
641 Nriagu, J. O.: A global assessment of natural sources of atmospheric trace metals.
642 Nature, 338, 47-49, doi:10.1038/338047a0, 1989.
643 Patil, R. S., Kumar, R., Menon, R., Shah, M. K., and Sethi, V.: Development of
644 particulate matter speciation profiles for major sources in six cities in India.
645 Atmos. Res., 132-133, doi:10.1016/j.atmosres.2013.04.012, 2013.
646 Perry, K. D., Chahill, T. A., Schnell, R. C., and Harris, J. M.: Long-range transport of
647 anthropogenic aerosols to the National Oceanic and Atmospheric Administration
648 baseline station at Mauna Loa Observatory, Hawaii. J. Geophys. Res. Atmos., 104
649 18521-18533, doi:10.1029/1998JD100083, 1999.
650 Pochanart, P., Akimoto, H., Kajii, Y., and Sukasem, P.: Carbon monoxide,

651 regional-scale, and biomass burning in tropical continental Southeast Asia:
652 Observations in rural Thailand. J. Geophys. Res. Atmos., 108, D17,
653 doi:10.1029/2002JD003360, 2003.
654 Ramanathan, V., Crutzen, R. J., Kiehl, J. T., and Rosenfeld, D.: Aerosols, climate and
655 the hydrological cycle. Science, 294, 2119-2124, doi:10.1126/science.1064034,
656 2001.
657 Roberts, L. C., Hug, S. J., Dittmar, J., Voegelin, A., Kretzschmar, R., Wehrli, B.,
658 Cirpka, O. A., Saha, G. C., Ali, M. A., and Badruzzaman, A. B. M.: Arsenic
659 release from paddy soils during monsoon flooding. Nat. Geosci. 3, 53-59,
660 doi:10.1038/ngeo723, 2010.
661 Stress, D. G., Yarber, K. F., Woo, J.-H., and Carmichael, G. R.: Biomass burning in
662 Asia: Annual and seasonal estimates and atmospheric emissions. Global
663 BiogeoChem. Cycles 170, 1099, doi:10.1029/2003GB002040, 2003.
664 Tang, Y., Carmichael, R. G., Woo, J.-H., Thongboonchoo, N., Kurata, G., Uno, I.,
665 Streets, D. G., Blake, D. R., Weber, R. J., Talbot, R. W., Kondo, Y., Singh, H. B.,
666 and Wang, T.: Influence of biomass burning during the Transport and Chemical
667 Evolution Over the Pacific (TRACE-P) experiment identified by the regional
668 chemical transport model. J. Geophys. Res. Atmos., 108, D21,
669 doi:10.1029/2002JD003110, 2003
670 Taylor, S. R.: Abundance of chemical elements in the continental crust: a new table.
671 Geochim. Cosmochim. Acta, 28, 1273-1285, doi:10.1016/0016-7037(64)90129-2,
672 1964.
673 Val Martin, M., Logan, J. A., Kahn, R., Leung, F., Nelson, D. L., Diner, D.: Smoke
674 injection heights from fires in North America: analysis of 5 years of satellite
675 observations. Atmos. Chem. Phys., 10, 1491-1510,

doi:10.5194/acp-10-1491-2010.

ven der Werf, G. R., Randerson, J. T., Giglio, L., van Leeuwen, T. T., Chen, Y., Rogers, B. M., Mu, M., van Marie, M. J. E., Morton, D., Collatz, G. J., Yokelson, R. J., Kasibhatla, P. S., 2017. Global fire emissions estimates during 1997-2016. Earth Syst. Sci. Data, 9, 697-720, doi:10.5194/essd-9-697-2017.

Venter, A. D., van Zyl, P. G., Beukes, J. P., Josipovic, M., Hendriks, J., Vakkari, V., Laakso, L., Atmospheric trace metals measured at a regional background site, (Welgegund) in South Africa. Atmos. Chem. Phys., 17, 4251-4263, doi:10.5194/acp-17-4251-2017, 2017.

Viana, M., Querol, X., Alastuey, A., Gil, J. J., Menéndez, M., Identification of PM sources by principal component analysis (PCA) coupled with wind direction data. Chemosphere, 65, 2411-2418, doi:10.1016/j.chemosphere.2006.04.060, 2006.

Wai, K.-H., Wu, S., Li, X., Jaffe, D. J., and Perry, K.D.: Global atmospheric transport and source-receptor relationships for arsenic. Environ. Sci. Technol., 50, 3714-3720, doi:10.1021/acs.est.5b05549, 2016.

Walsh, P. R., Duce, R. A., and Fasching, J. L.: Considerations of the enrichment, sources and flux of arsenic in the troposphere. J. Geophys. Res. Oceans, 84, 1719-1726, doi:10.1029/JC084iC04p01719, 1979.

Weiss-Penizas, P, Jaffe, D., Swartzendruber, P., Hafner, W., Chand, D., and Prestbo, E.: Quantifying Asian and biomass burning sources of mercury using the Hg/CO ratio in pollution plumes observed at the Mount Bachelor observatory. Atmos. Environ., 41, 4366-4379, doi:10.1016/j.atmosenv.2007.07.058, 2007.

Zieman, J. J., Holmes, J. L., Connor, D., Jensen, C. R., Zoller, W. H.: Atmospheric aerosol trace element chemistry at Mauna Loa Observatory: 1. 1979-1985. J. Geophys. Res. Atmos., 100, 25979-25994, doi:10.1029/93JD03316, 1995.

Table Captions

Table 1 Summarizes of principal component analysis for aerosol species along with carbon monoxide observed at Mount Hehuan. Factor loadings lower than ± 0.4 are not given. Factor loadings lower than ± 0.7 are marked in bold.

Table 2 The max, min, mean, standard deviation values of As, Pb, K^+ and CO of on the BB and Non-BB days in RA and SA air clusters during the SE and S Asian BB periods (from January to May).

Figure Captions

Figure 1 Clusters of backward trajectory at Mount Hehuan from September 2011 to September 2012.

Figure 2 Monthly distributions of the fractions for various air clusters at Mount Hehuan during the sampling period.

Figure 3 Average concentrations of chemical compositions in TSP samples collected at Mount Hehuan site from September 2011 to September 2012.

Figure 4 Monthly distributions of 5th, 25th, 50th, 75th and 95th percentile values of As concentrations observed at Mount Hehuan from 2011 September to 2012 September.

Figure 5 Scattered plots of As against (a) K^+, (b) Al and (c) Pb in different As concentration bins observed at Mount Hehuan

Figure 6 Time series of daily airborne particulate As, Pb and K^+ along with CO concentrations and clusters of trajectory observed from January to May in 2012. In the bottom panel. the green and grey crosses denote BB and non-BB samples identified in the text.

Figure 7 MODIS fires on ground surface and WRF-Chem modeled results of BB plumes at the altitude of 700 hPa on (a) April 3 and (b) March 15. The blue arrows and lines denote the wind direction and wind speed, respectively. The grey shadows represent tracer concentrations.

Figure 8 Scattered plots of As against K^+ observed at Mount Hehuan in (a) SA, (b) SEA and (c) other air groups during the S Asian biomass burning seasons.

Figure 9 Scattered plots of As against Pb observed at Mount Hehuan in (a) SA, (b) SEA and (c) other air groups during the S Asian biomass burning seasons.

Table 1 Summarizes of principal component analysis for aerosol species along with carbon monoxide observed at Mount Hehuan. Factor loadings lower than ± 0.4 are not given. Factor loadings lower than ± 0.7 are marked in bold.

	BB periods (from January to May)			**Non-BB periods (from June to December)**		
Components	PC1	PC2	PC3	PC1	PC2	PC3
Al	**0.96**	-	-	**0.98**	-	-
Fe	**0.96**	-	-	**0.97**	-	-
Mg	**0.90**	-	-	**0.73**	-	-
Ca	**0.87**	-	-	**0.71**	-	-
Sr	**0.87**	-	-	-	-	-
Ba	**0.94**	-	-	**0.85**	-	-
Ti	**0.97**	-	-	**0.97**	-	-
Mn	**0.97**	-	-	**0.81**	0.48	-
Ni	**0.96**	-	-	-	-	-
Zn	**0.85**	-	-	-	-	-
Mo	**0.84**	-	-	-	0.40	-
Sb	**0.76**	0.55	-	-	**0.89**	-
Tl	**0.85**	0.43	-	-	**0.87**	-
Pb	-	0.51	-	-	0.45	-
V	**0.98**	-	-	**0.75**	0.47	-
As	-	0.67	-0.44	-	**0.80**	-
Se	**0.87**	0.43	-	-	**0.85**	-
Rb	**0.98**	-	-	**0.91**	-	-
La	**0.94**	-	-	**0.94**	-	-
Ce	**0.95**	-	-	**0.95**	-	-
Nd	**0.96**	-	-	**0.97**	-	-
Na^+	**-**	-	**0.80**	-	-	**0.87**
NH_4^+	**0.80**	0.49	-	-	-	**0.78**
K^+	**-**	**0.71**	0.47	-	-	**0.68**
Cl^-	**-**	-	**0.66**	-	-	**0.70**
SO_4^{2-}	**0.86**	0.47	-	-	0.53	**0.73**
$NO3^-$	**0.75**	-	0.55	-	-	**0.79**
CO	0.43	0.50	-	-	0.59	-
Potential sources	Dust + SIA + Industry	BB	Sea salt	Dust	Industry	SIA + Sea salt
Explain variance	49.3	25.9	16.1	34.9	17.4	16.2

Table 2 The max, min, mean, standard deviation values of As, Pb, K^+ and CO of on the BB and Non-BB days in RA and SA air clusters during the SE and S Asian BB periods (from January to May).

Categories	As ($ng\ m^{-3}$)	Pb ($ng\ m^{-3}$)	K^+ ($ng\ m^{-3}$)	CO (ppb)
SA air cluster				
Non-BB				
Max	3.5	16.9	831	432
Min	0.05	0.6	15	102
Mean	0.6	4.5	207	188
Std.	0.7	3.8	173	86
BB				
Max	5.3	28.5	1617	316
Min	0.13	1.6	71	156
Mean	1.6	10.2	404	217
Std.	1.4	7.3	336	42
Differences[1]	1.0	5.7	197	29
SEA air cluster				
Non-BB				
Max	1.6	10.0	452	282
Min	0.02	0.3	4	95
Mean	0.4	2.9	151	148
Std.	0.4	2.5	141	45
BB				
Max	2.3	11.0	609	259
Min	0.08	1.1	139	170
Mean	0.6	4.2	328	212
Std.	0.7	3.2	178	39
Differences	0.2	1.3	177	64

1. Difference for each species are calculated by the mean values in BB and non-BB events.

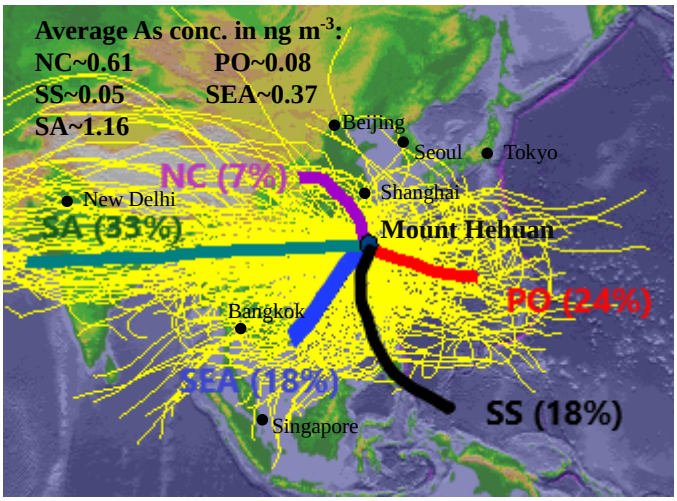
Average As conc. in ng m-3:
NC~0.61
PO~0.08
SS~0.05
SEA~0.37
SA~1.16
Beijing
Seoul
Tokyo
NC (7%)
New Delhi
Shanghai
SA (33%)
Mount Hehuan
PO (24%)
Bangkok
SEA (18%)
SS (18%)
Singapore

Figure 1

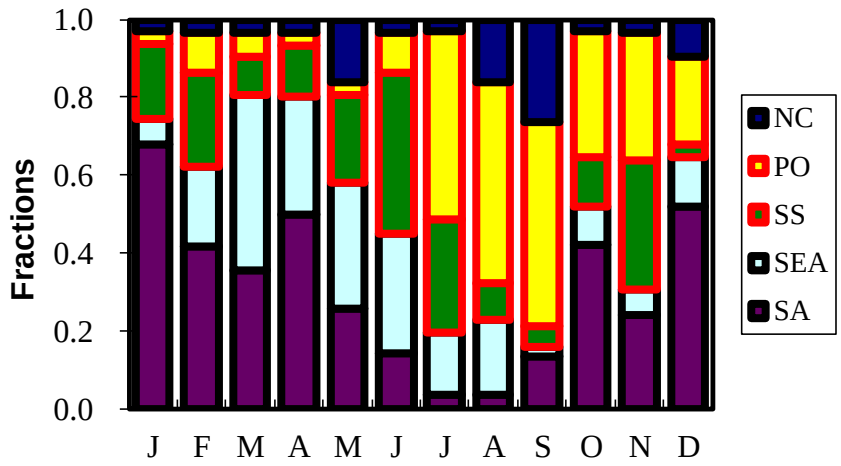

Figure 2

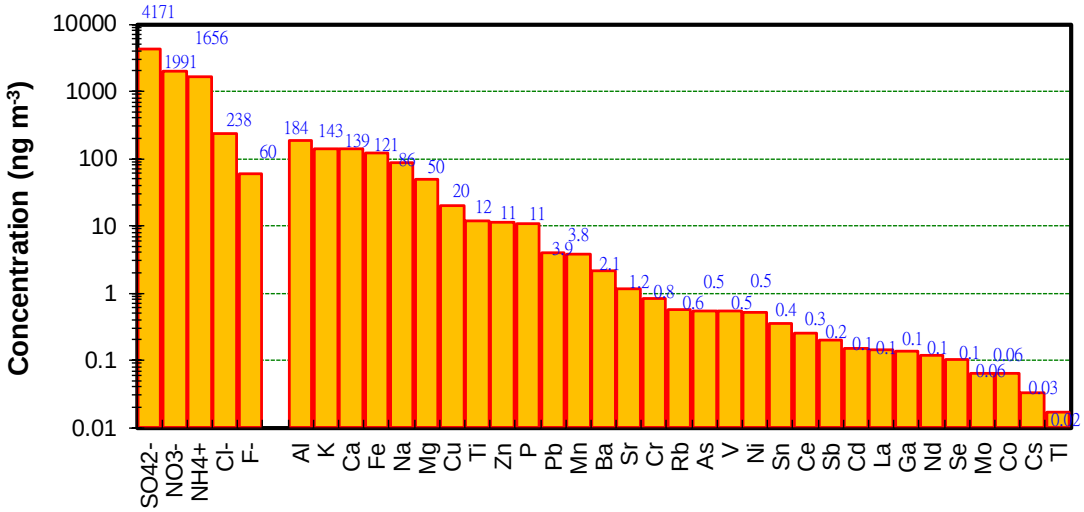
Concentration (ng m-3)
10000
1000
100
10
1
0.1
0.01
4171
1991
1656
238
60
184
143
139
121
86
50
20
12
11
11
3.9
3.8
2.1
1.2
0.8
0.6
0.5
0.5
0.5
0.4
0.3
0.2
0.1
0.1
0.1
0.1
0.1
0.06
0.06
0.03
0.02
SO42-
NO3-
NH4+
Cl-
F-
Al
K
Ca
Fe
Na
Mg
Cu
Ti
Zn
P
Pb
Mn
Ba
Sr
Cr
Rb
As
V
Ni
Sn
Ce
Sb
Cd
La
Ga
Nd
Se
Mo
Co
Cs
Tl

Figure 3

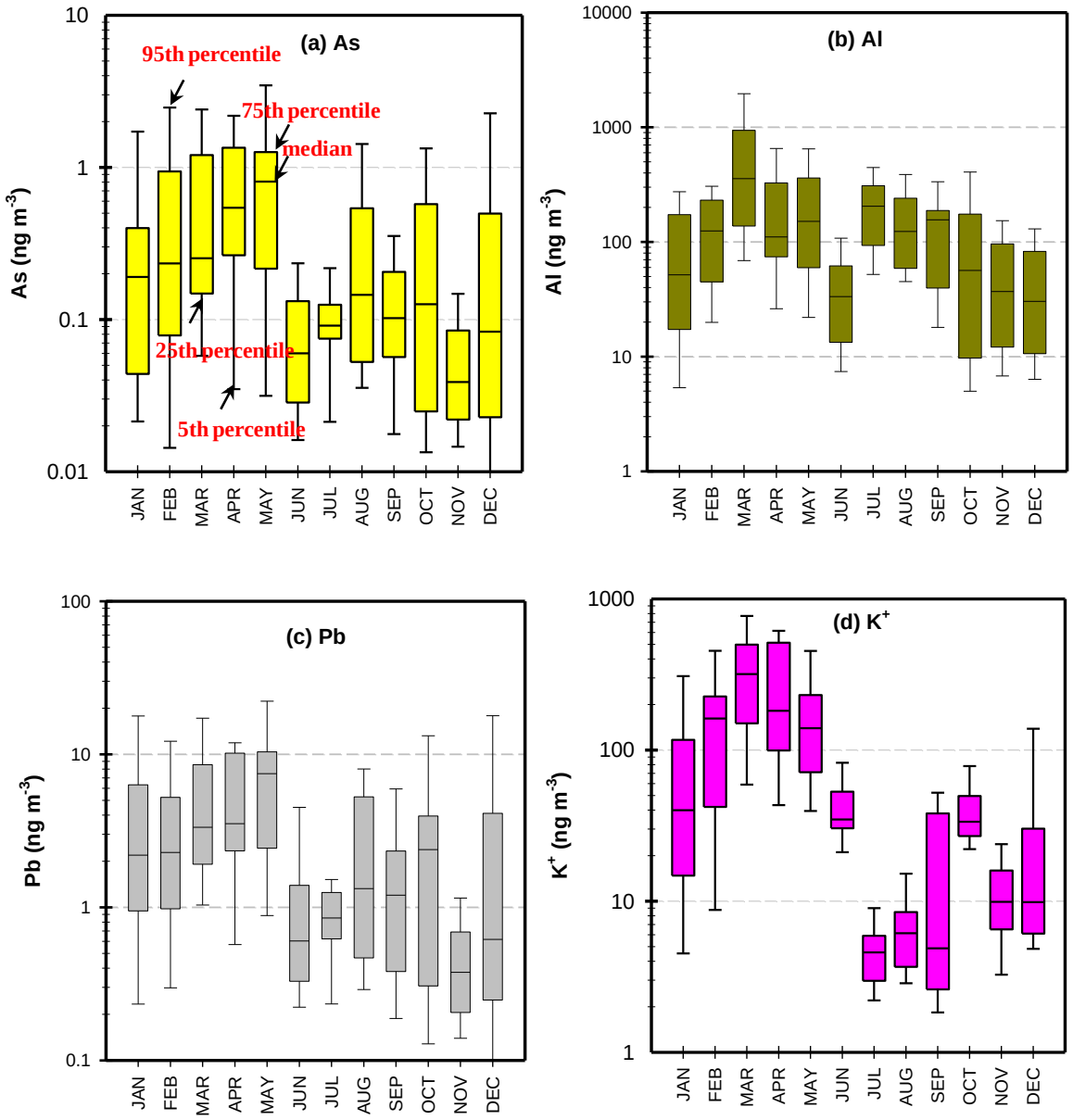
(a) As
95th percentile
75th percentile
median
25th percentile
5th percentile
As (ng m-3)
10
1
0.1
0.01
(b) Al
Al (ng m-3)
10000
1000
100
10
1
(c) Pb
Pb (ng m-3)
100
10
1
0.1
(d) K+
K+ (ng m-3)
1000
100
10
1
JAN
FEB
MAR
APR
MAY
JUN
JUL
AUG
SEP
OCT
NOV
DEC

Figure 4

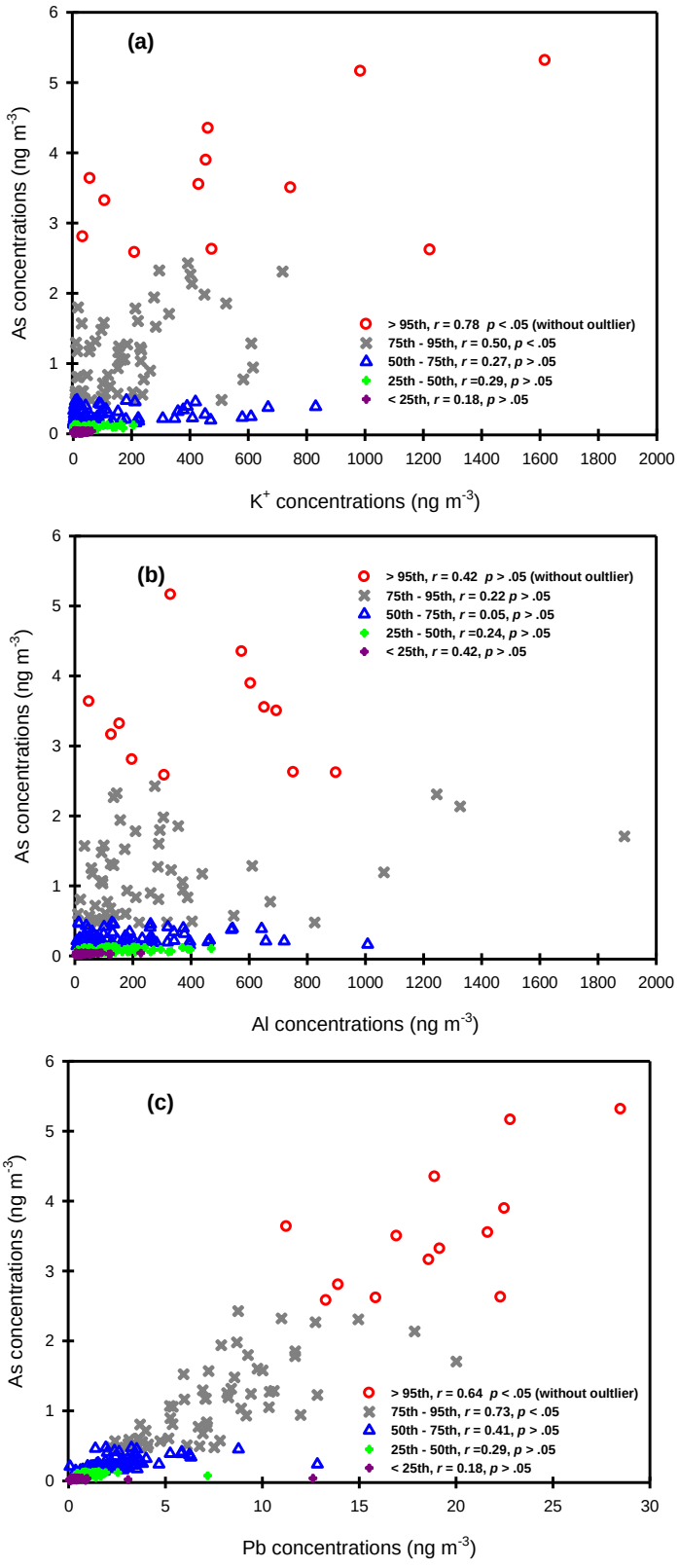
(a)
As concentrations (ng m-3)
K+ concentrations (ng m-3)
> 95th, r = 0.78 p < .05 (without oultlier)
75th - 95th, r = 0.50, p < .05
50th - 75th, r = 0.27, p > .05
25th - 50th, r =0.29, p > .05
< 25th, r = 0.18, p > .05
(b)
As concentrations (ng m-3)
Al concentrations (ng m-3)
> 95th, r = 0.42 p > .05 (without oultlier)
75th - 95th, r = 0.22 p > .05
50th - 75th, r = 0.05, p > .05
25th - 50th, r =0.24, p > .05
< 25th, r = 0.42, p > .05
(c)
As concentrations (ng m-3)
Pb concentrations (ng m-3)
> 95th, r = 0.64 p < .05 (without oultlier)
75th - 95th, r = 0.73, p < .05
50th - 75th, r = 0.41, p > .05
25th - 50th, r =0.29, p > .05
< 25th, r = 0.18, p > .05

Figure 5

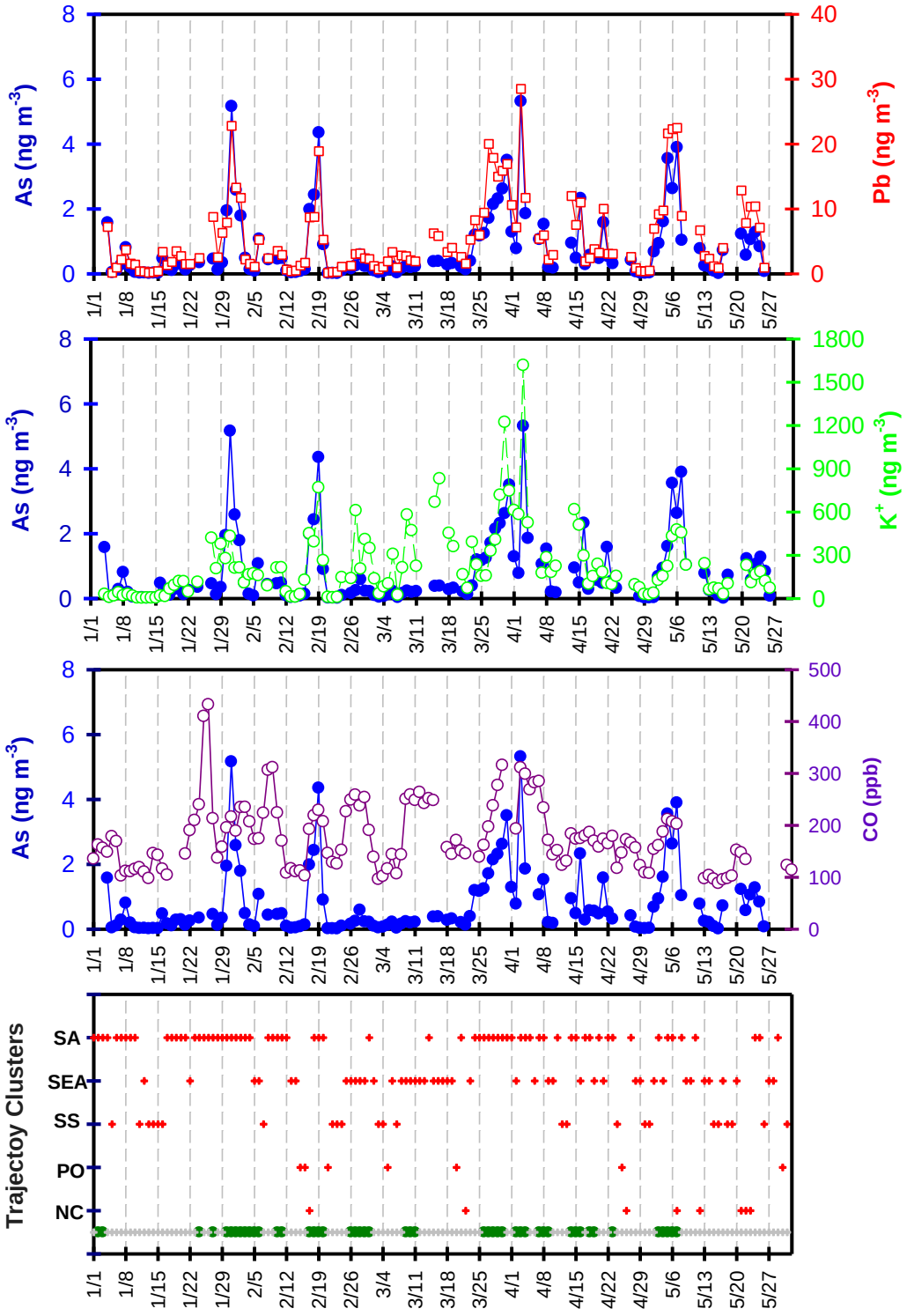
As (ng m-3)
Pb (ng m-3)
K+ (ng m-3)
CO (ppb)
Trajectoy Clusters
SA
SEA
SS
PO
NC
1/1
1/8
1/15
1/22
1/29
2/5
2/12
2/19
2/26
3/4
3/11
3/18
3/25
4/1
4/8
4/15
4/22
4/29
5/6
5/13
5/20
5/27

Figure 6

(a)

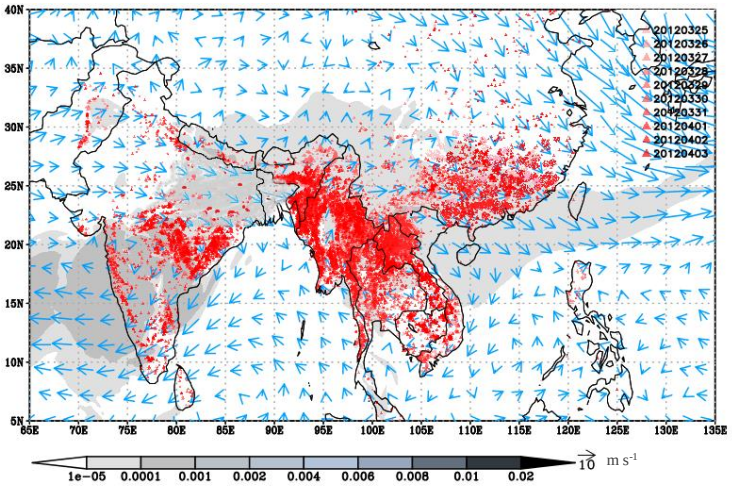
20120325
20120326
20120327
20120328
20120329
20120330
20120331
20120401
20120402
20120403
1e−05 0.0001 0.001 0.002 0.004 0.006 0.008 0.01 0.02
10 m s-1

(b)

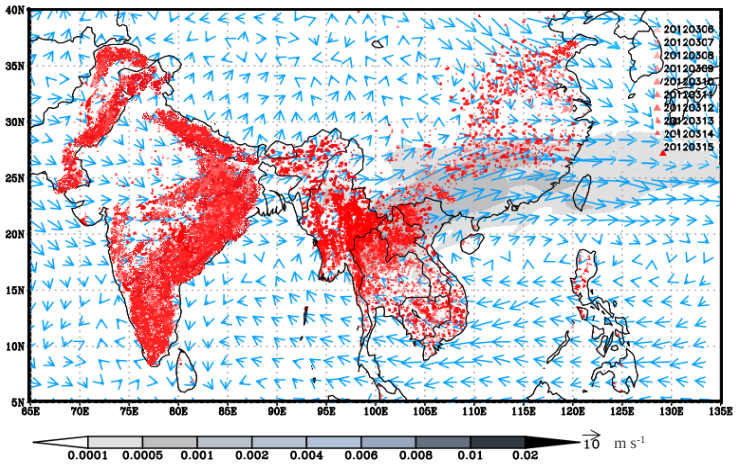
20120306
20120307
20120308
20120309
20120310
20120311
20120312
20120313
20120314
20120315
0.0001 0.0005 0.001 0.002 0.004 0.006 0.008 0.01 0.02
10 m s-1

Figure 7

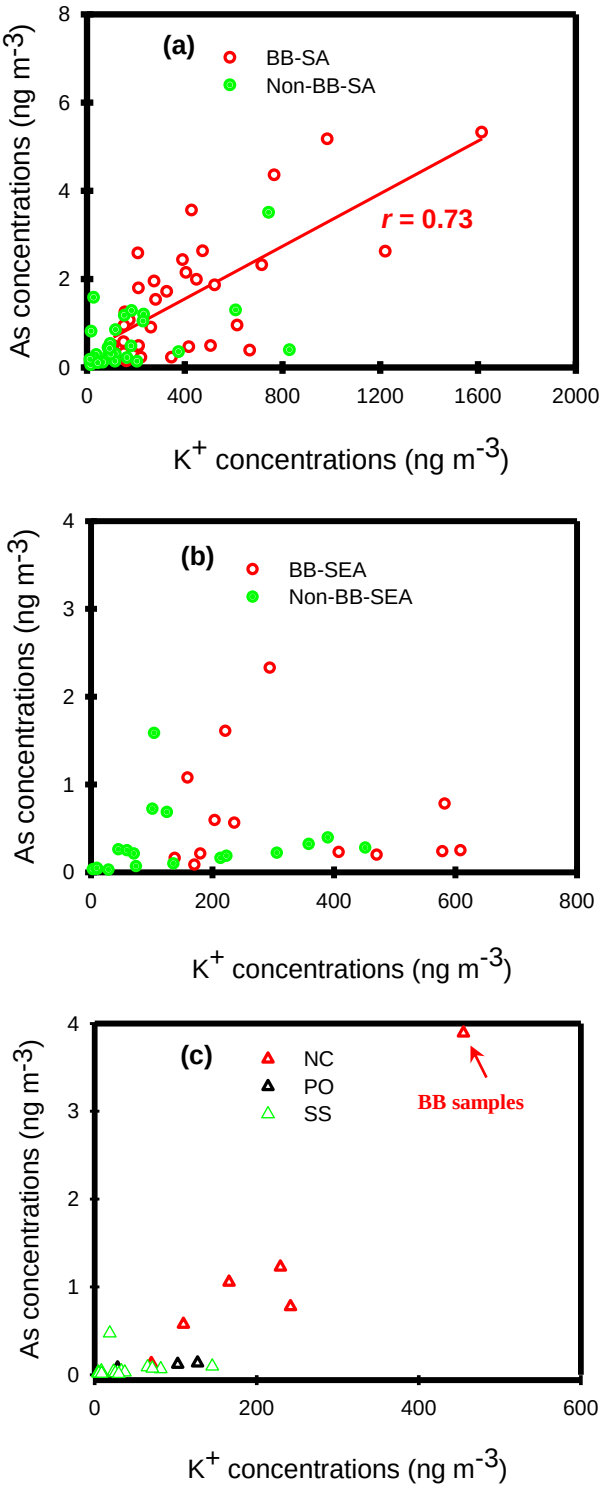
(a)
BB-SA
Non-BB-SA
r = 0.73
As concentrations (ng m-3)
K+ concentrations (ng m-3)
0
2
4
6
8
0
400
800
1200
1600
2000
(b)
BB-SEA
Non-BB-SEA
As concentrations (ng m-3)
K+ concentrations (ng m-3)
0
1
2
3
4
0
200
400
600
800
(c)
NC
PO
SS
BB samples
As concentrations (ng m-3)
K+ concentrations (ng m-3)
0
1
2
3
4
0
200
400
600

Figure 8

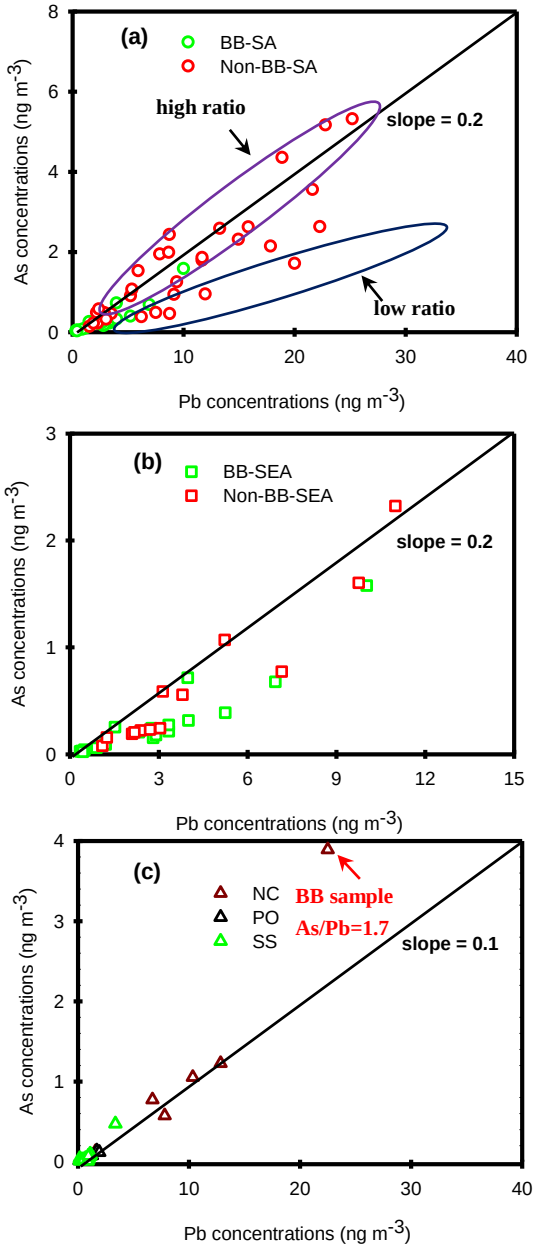
(a)
BB-SA
Non-BB-SA
high ratio
slope = 0.2
low ratio
As concentrations (ng m-3)
Pb concentrations (ng m-3)
(b)
BB-SEA
Non-BB-SEA
slope = 0.2
As concentrations (ng m-3)
Pb concentrations (ng m-3)
(c)
NC
PO
SS
BB sample
As/Pb=1.7
slope = 0.1
As concentrations (ng m-3)
Pb concentrations (ng m-3)

Figure 9